reactions

MDPI

Article

Photocatalytic Degradation Pathways of the Valsartan Drug by TiO_2 and g-C_3N_4 Catalysts

Feidias Bairamis [1] and Ioannis Konstantinou [1,2,*]

[1] Department of Chemistry, University of Ioannina, 45110 Ioannina, Greece; f.mpairamis@uoi.gr
[2] Institute of Environment and Sustainable Development, University Research Center of Ioannina (URCI), 45110 Ioannina, Greece
* Correspondence: iokonst@uoi.gr; Tel.: +30-26510-08349

Abstract: The photocatalytic degradation of the valsartan (VLS) pharmaceutical using TiO_2 and g-C_3N_4 catalysts under simulated solar light is studied in this paper by high-resolution Orbitrap mass spectrometry. $^{\bullet}OH$ radicals were the major oxidant species for the degradation of valsartan using TiO_2, while positive holes (h^+), followed by a much lesser amount of $^{\bullet}OH$ radicals, were the major species in the case of g-C_3N_4. Valsartan degradation followed first order kinetics by both catalysts with TiO_2 being the catalyst with the better photocatalytic efficiency. The transformation products (TPs) and their evolution profiles are identified and monitored, respectively, by means of LC-HRMS. Based on TPs identification, the degradation mechanisms are discussed. The major degradation pathways for g-C_3N_4 include decarboxylation and subsequent oxidation, hydroxylation, and cleavage of C–N bond, while for TiO_2 cyclization, TPs are abundant and the hydroxylation occurs in the first stage products. The study highlights the complex nature of TPs formed during such processes, the different mechanisms involved and the necessity for the identification of TPs for the assessment of the treatment and the tracking of such TPs in different environmental compartments.

Keywords: pharmaceuticals; valsartan; photocatalysis; oxidation pathways; TiO_2; g-C_3N_4

check for updates

Citation: Bairamis, F.; Konstantinou, I. Photocatalytic Degradation Pathways of the Valsartan Drug by TiO_2 and g-C_3N_4 Catalysts. *Reactions* **2022**, *3*, 160–171. https://doi.org/10.3390/reactions3010012

Academic Editors: Hugo de Lasa and Dmitry Yu. Murzin

Received: 10 December 2021
Accepted: 1 February 2022
Published: 3 February 2022

1. Introduction

During the last few years, the studies on the fate and transformation of pharmaceutical compounds are gaining scientific attention because of their continuous occurrence and increasing concentrations in different types of water, such as wastewater, surface water, ground water and even drinking water [1–5]. Valsartan (VAL) is an Angiotensin II receptor antagonist belonging to the commonest antihypertensive drugs [6,7]. As a result, high concentration levels of VAL in different types of water have been reported in several previous studies around the world. As example, the median and maximum concentration of VAL in surface waters from 33 European countries was 1507 and 7479 ng/L, respectively [8]. In addition, according to the studies of Castro et al. [9] and Peña Guzman et al. [10], maximum concentrations of VAL observed in wastewaters for Spain and 11 countries of Latin America were 9986 ng/L and 1900 ng/L, respectively. Finally, the presence of Valsartan in raw, secondary treated wastewaters and surface waters has been previously reported in our previous studies [11,12].

Because of this widespread occurrence of pharmaceutical residues, such as VLS, in different systems and the possible adverse effects that can exert in different organisms, advanced treatment technologies should be applied for environmental protection. Advanced oxidation processes (AOPs) have earned the attention because they can degrade/mineralize biorecalcitrant pollutants in short times. In addition, they can be applied to simulate oxidation processes in environmental media. Semiconductor photocatalysis is one of the most studied processes among AOPs with TiO_2 being by far the most studied catalyst because of its chemical and photochemical stability, low cost and high photocatalytic performance.

However, the photocatalytic activity of TiO_2 using solar light is limited, because of its band gap (3.0–3.2 eV) [13,14]. g-C_3N_4, an alternative and promising polymeric semiconductor photocatalyst with visible light response (band gap 2.7 eV), has gained attention in recent years. This metal-free catalyst with a two-dimensional (2D) nanostructure demonstrates high thermal (up to 600 °C, in air) and chemical stability in acidic and basic media due to its s-triazinic structure, while it is insoluble in common solvents (ethanol, DMF, water) [15,16].

To date, very few studies performed lately deals with valsartan degradation in aqueous matrices by AOPs, i.e., by persulfate activation via sulfate radicals [17], photo-electro-Fenton [18], sonochemical degradation [19] and ozonation [20]. Some of these studies focused on the process parameters, while few data on the identification of degradation products are available. As a result, there is a lack of data concerning the heterogeneous semiconductor photocatalytic degradation of VLS in aquatic media.

Based on the above, the photocatalytic degradation of VAL by TiO_2 (P25) and graphitic carbon nitride (g-C_3N_4) catalysts in aqueous suspensions is studied in the present study. The particular aims of the present work are: (a) the application of heterogeneous photocatalysis using TiO_2 and g-C_3N_4 under simulated solar light for the removal of valsartan residues from water matrices, a topic that has not been investigated to date; (b) The identification of transformation products via the powerful instrumentation of ultra-performance liquid chromatography combined with high resolution and accurate mass linear ion trap-orbitrap mass spectrometer (UPLC—LIT–Orbitrap-MS); (c) the elucidation of transformation pathways by two different oxidant species, $^{\bullet}OH$ radicals and positive holes (h^+).

2. Results and Discussion

2.1. Preliminary Experiments

Valsartan photocatalytic degradation kinetics using TiO_2 and g-C_3N_4 catalysts are presented in Figure 1, while the linear transformation plot (natural logarithm of normalized concentration against irradiation time) is shown in the figure inset. Pseudo-first order kinetics were observed in both TiO_2 and g-C_3N_4 cases ($R^2 > 0.979$ and $R^2 > 0.9927$) with 0.205 min^{-1} and 0.028 min^{-1} being the corresponding reaction rate constants. The degradation of valsartan in the dark followed very slow kinetics ($k = 0.0003$ min^{-1}), while photolysis ($k = 0.0059$ min^{-1}) under the same irradiation conditions was also a much slower process than photocatalysis.

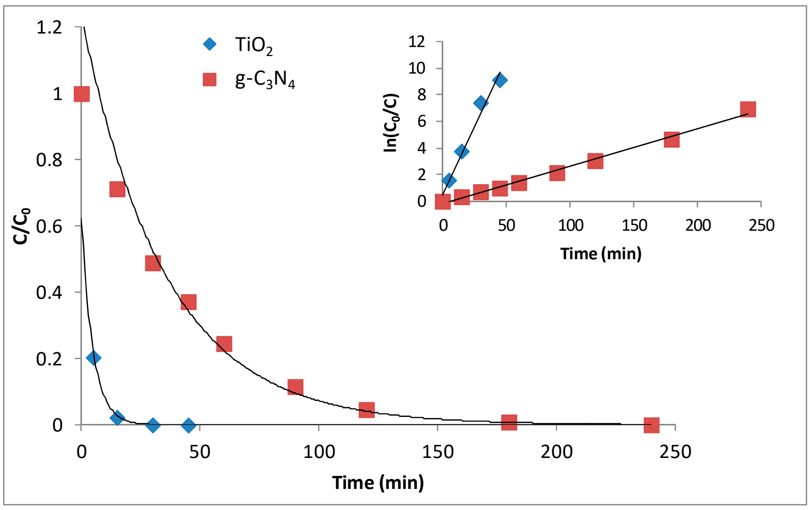

Figure 1. Photocatalytic degradation kinetics of valsartan by TiO_2 and g-C_3N_4 catalysts ((valsartan) = 5 mg L^{-1}; (catalyst) = 100 mg L^{-1}; I = 500 Wm^{-2}).

The concentrations of $^{\bullet}OH$ radicals generated by TiO_2 and g-C_3N_4 catalysts, as determined by the hydroxy-terephthalic acid fluorescence method (Figure 2), were 22.4 µM and 0.32 µM, respectively. The above results are consistent with the catalysts conduction band energy levels, showing that TiO_2 photocatalytic degradation proceeded mainly through the generation of hydroxyl radicals, while g-C_3N_4 photocatalytic degradation proceed mainly through the positive holes and only a small amount of $^{\bullet}OH$ radicals was formed, probably through the oxygen reduction pathway with the sequential formation of superoxide radical anion, hydrogen peroxide and finally $^{\bullet}OH$ radicals. E_{VB} and E_{CB} of g-C_3N_4 were calculated at 1.58 eV and −1.24 eV, respectively while the $OH^-/^{\bullet}OH$ and $O_2/O_2^{\bullet-}$ potentials are 2.4 and −0.33 eV, respectively.

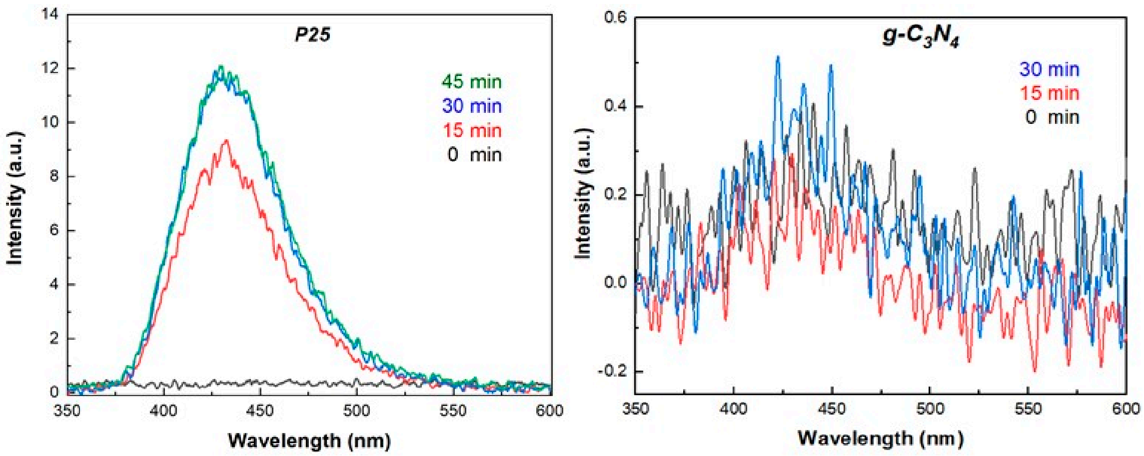

Figure 2. Fluorescence spectra intensity of hydroxy-terephthalic acid (OHTA) formation by TiO_2 and g-C_3N_4, ((catalyst) = 100 mg L^{-1}; I = 500 Wm^{-2}).

2.2. Photocatalytic Transformation Products and Pathways of Valsartan by UV-Vis/g-C_3N_4 Process

LC–HRMS identification data of VLS TPs by g-C_3N_4 photocatalysis are summarized in Table 1. Firstly, the parent compound (VLS) and sodium adduct $[M + Na]^+$ were observed at m/z 436.2336 ($C_{24}H_{30}O_3N_5^+$) and 458.2145 ($C_{24}H_{29}O_3N_5Na^+$), respectively, while MS^2 and MS^3 fragments are closely identical to those reported elsewhere [18]. In addition, VLS showed also a pseudo-molecular ion $[M-H]^-$ at m/z 434.2194 ($C_{24}H_{28}O_3N_5$) in the negative ionization mode due to the presence of the carboxylic acid functional group. The screening of TPs performed under negative ESI ionization can be used as an indicative tool for the presence of the carboxylic acid group in the structure of TPs.

Positive holes (h^+) react principally with the electron-rich moieties of organic substances via electron transfer [21]. In the case of valsartan, such electron-rich functional group sites are the phenyl and tetrazole moieties as well as the carboxylic acid and tertiary amine groups. TP1, with $[M + H]^+/[M + Na]^+$ at m/z 392.22437/414.2253, respectively, differs 44 amu less than the parent drug and the matching chemical formula ($C_{23}H_{30}ON_5^+$) indicates clearly the loss of CO_2 group. The formation of TP1 can be rationalized through a photo-Kolbe decarboxylation according to the following equation:

$$RCOO^- + h^+ \rightarrow R^{\bullet} + CO_2 \tag{1}$$

TP2 with $[M + H]^+$ at m/z 406.2227 and a chemical formula $C_{23}H_{30}ON_5^+$, having a difference of 14 amu from TP1, was assigned to a ketone derivative. In addition, TP5 with $[M + H]^+$ at m/z 364.1759 and a chemical formula $C_{20}H_{22}O_2N_5^+$ presented characteristic MS^2/MS^3 fragments that showed that the biphenyl-tetrazole and valeryl groups were intact. Similarly, TP6 with $[M + H]^+$ at m/z 336.1810 and a chemical formula $C_{19}H_{22}ON_5^+$ was assigned to N-((2′-(1H-tetrazol-5-yl)biphenyl-4-yl)methyl) pentanamide. The alkyl radical formed after decarboxylation can react rapidly with molecular oxygen, leading to the formation of peroxy radical. Peroxy radicals are disproportionate to alcohols and ketones via the Russell and/or Bennet–Summers mechanisms [22], but also form alkoxy radicals that lead to aldehyde, as well as fragmentation to form new alkyl radicals [23]. The formation of TP2, TP5 and TP6 can be rationalized by the above-mentioned mechanisms. Based on the TPs profile (Figure 3), the peak concentrations of the above products were observed in the same time framework; thus, it can be considered that took place concurrently.

Table 1. UPLC-ESI-HR-MS data (pseudo-molecular ions $(M + H)^+$ or $(M - H)^-$ */$(M + Na)^+$; chemical formula; mass error Δ(ppm); and ring-double\bond equivalents, RDB) for VLS and transformation products by g-C_3N_4 photocatalytic oxidation.

VLS/TPs	$(M + H)^+/(M + Na)^+$ $(M - H)^-$*	Formula	Δ(ppm)	RDB
VLS	436.2336 458.2145	$C_{24}H_{30}O_3N_5$ $C_{24}H_{29}O_3N_5Na$	−1.619	12.5
GCN-TP1	392.2437 414.2253	$C_{23}H_{30}ON_5$ $C_{23}H_{29}ON_5Na$	−2.083	11.5
GCN-TP2	406.2227 428.2045	$C_{23}H_{28}O_2N_5$ $C_{23}H_{27}O_2N_5Na$	−2.712	12.5
GCN-TP3	450.2148 *	$C_{24}H_{28}O_4N_5$	2.664	13.5
GCN-TP4	450.2144 *	$C_{24}H_{28}O_4N_5$	−0.506	13.5
GCN-TP5	364.1759 386.1574	$C_{20}H_{22}O_2N_5$ $C_{20}H_{21}O_2N_5Na$	−2.475	12.5
GCN-TP6	336.1810 358.1628	$C_{19}H_{22}ON_5$ $C_{19}H_{21}ON_5Na$	−2.727	11.5
GCN-TP7	356.1341 378.1161	$C_{17}H_{18}O_4N_5$ $C_{17}H_{17}O_4N_5Na$	−3.483	11.5
GCN-TP8	267.0868 289.0685	$C_{14}H_{11}O_2N_4$ $C_{14}H_{10}O_2N_4Na$	−3.228	11.5
GCN-TP9	400.1238 422.1057	$C_{18}H_{18}O_6N_5$ $C_{18}H_{17}O_6N_5Na$	−3.523	12.5
GCN-TP10	202.1433 224.1249	$C_{10}H_{20}O_3N$ $C_{10}H_{19}O_3NNa$	−2.523	1.5

Alternatively, the attack of holes to phenyl moieties via the electron transfer mechanism may lead to the generation of an unstable carbon-centered cationic radical that is subsequently hydrolyzed to produce the corresponding hydroxy derivative, OH-VLS. In the same way, the attack to the tetrazole moiety can lead also to the formation of a hydroxy analogue. TP3 and TP4 with $[M - H]^-$ at m/z 450.2148 and 450.2144, respectively, and a chemical formula $C_{24}H_{28}O_4N_5^-$, differing 16 amu from VLS, were attributed to the hydroxy derivatives of VLS. Taking into account the MS^2/MS^3 characteristic fragments, the suggested hydroxylation position is on biphenyl or tetrazole ring. In a VAL sonochemical oxidation study, an $^{\bullet}$OH-based process, Serna-Galvis and co-workers [19] identified four hydroxy-TPs of VLS at phenyl, tetrazole and valeryl functional groups. The similar hydroxylation pathway may be applied for the first stage generated products leading to the formation of secondary TPs, such as TP9 and TP7 as justified also by their evolution profiles (Figure 3). TP7 presented $[M + H]^+$ at m/z 356.1341 and $C_{17}H_{18}O_4N_5^+$ chemical formula, while TP9 presented $[M + H]^+$ at m/z 400.1238 and $C_{18}H_{18}O_6N_5^+$ as a chemical formula.

One-electron oxidation of tertiary amine group yielding a nitrogen centered cation radical [24] can represent another degradation pathway. This intermediate cation radical is subsequently subjected to C–N cleavage to generate transformation products TP10 and TP8 with concurrent hydroxylation. TP10 presented $[M + H]^+$ m/z 202.1433 ($C_{10}H_{20}O_3N^+$), $[M + Na]^+$ m/z 224.1249 ($C_{10}H_{19}O_3NNa^+$), while TP8 presented $[M + H]^+$ m/z 267.0868, $C_{14}H_{11}O_2N_4^+$. TP10 has been also previously detected along photo-electro-Fenton degradation of VLS (Martínez-Pachón et al. 2018). No significant removal of TOC was observed in the presence of g-C_3N_4, which, in addition to the slower degradation rates of TPs, could be probably due to the partial dissolution or presence of g-C_3N_4 nanoparticles.

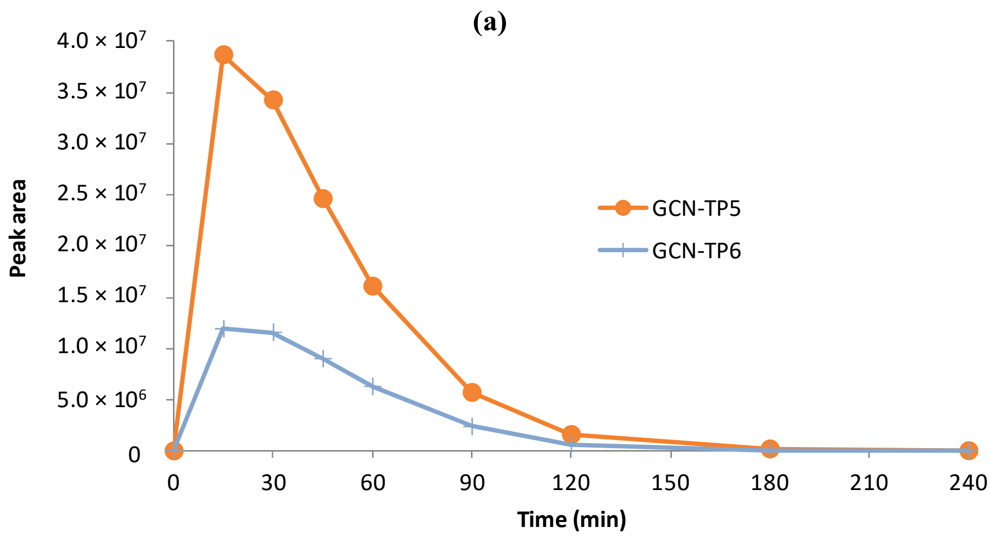

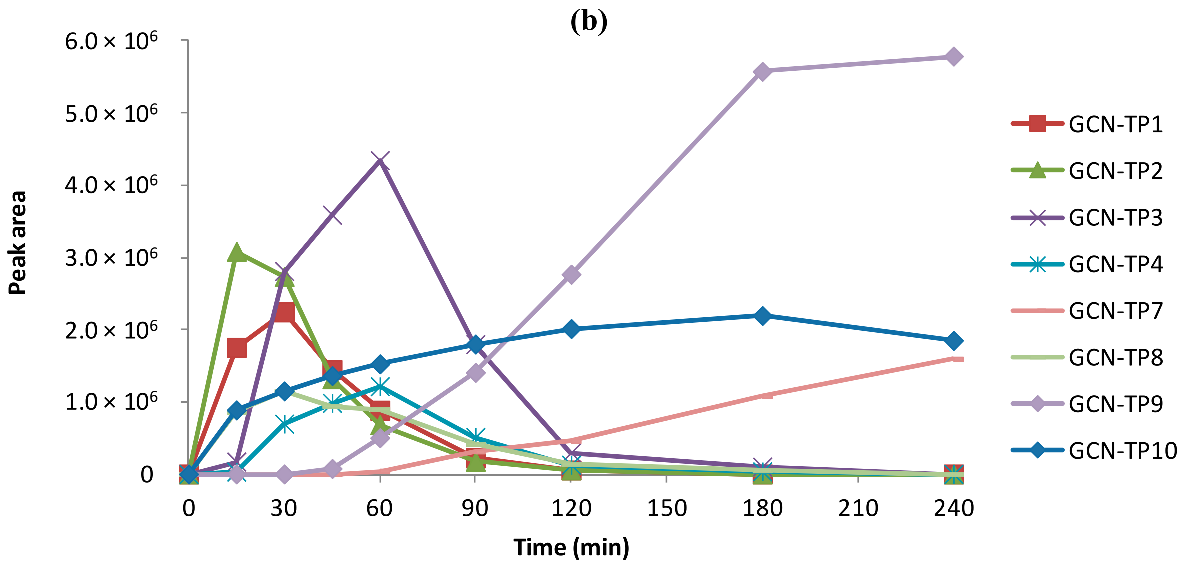

Figure 3. Evolution profiles of major (**a**) and minor (**b**) VLS TPs by g-C_3N_4 photocatalytic oxidation process.

Based on the mass spectra maximum intensities, the formation of TPs followed the sequence TP5 > TP6 > TP9 > TP3 > TP2 > TP1 > TP10 ≥ TP7,TP8,TP4, while the time interval for the formation of maximum concentration followed the trend TP5, TP6, TP1, TP2 (15–30 min) < TP4,TP3 (60 min) < TP7, TP9, TP10 (180–240 min). As a result, decarboxylation and further oxidation can be regarded as the major path, while hydroxylation and C–N cleavage may be considered as secondary paths. Based on the identification of TPs, as described previously, as well as on the TPs evolution kinetics, the tentative transformation pathways are summarized in Figure 4. In conclusion, VLS degradation by the g-C_3N_4 photocatalytic oxidation process followed three major pathways (Figure 4): (a) decarboxylation with further oxidation; (b) biphenyl or tetrazole moiety hydroxylation; and (c) rupture of the C–N bond in the tertiary amine group.

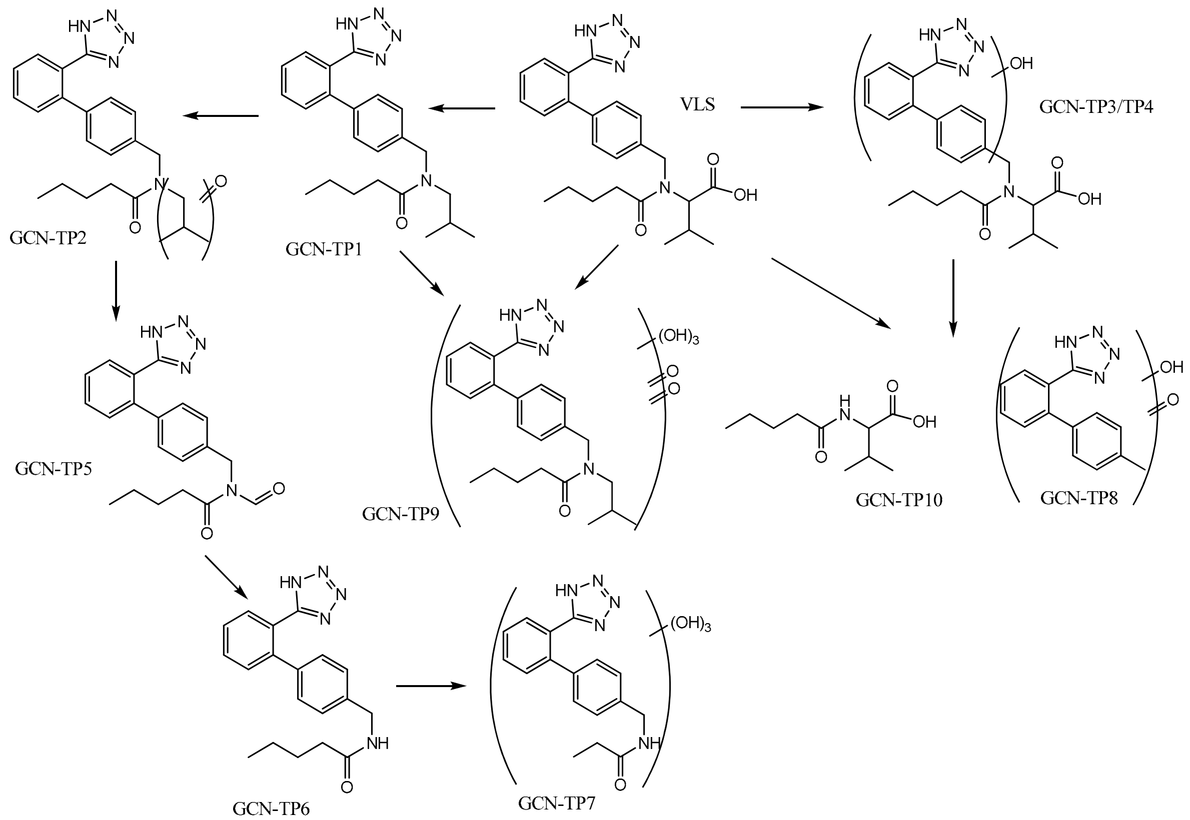

Figure 4. Proposed degradation pathways of valsartan by the g-C_3N_4 photocatalytic oxidation.

2.3. Photocatalytic Transformation Products and Pathways of Valsartan by UV-Vis/TiO_2 Process

LC–HRMS data on the identification of VLS TPs by TiO_2 photocatalysis are summarized in Table 2, while the respective chromatograms are depicted in Figure 5. TiO_2 photocatalytic oxidation is based on $^{\bullet}OH$ radicals, which react preferably with the electron-rich groups of organic substances via addition/elimination pathways, H-abstraction, and electron transfer [21]. The $^{\bullet}OH$ additions to aromatic moieties or unsaturated bonds compete overwhelming to H-abstraction. Electron transfer with $^{\bullet}OH$ is limited to very electron rich systems. In the case of valsartan, such electron-rich functional groups are the phenyl and tetrazole moieties. For tetrazole, $^{\bullet}OH$ radicals react at the -NH position either by electron transfer or H-abstraction [25]. The oxidation of primary, secondary, and tertiary aliphatic carbons is initiated by hydrogen atom abstraction forming a carbon-centered radical. The stabilization of such carbon-centered radicals can lead to the addition of molecular oxygen to form peroxy radicals, which subsequently yield the corresponding oxidation products as mentioned previously. Moreover, for the N-methylated amide function, abstraction by $^{\bullet}OH$ radicals takes place mainly from the N-methyl group [26]. Finally, the reaction of carboxylic acids (i.e., 2-methylbutanoic acid group of VLS) with $^{\bullet}OH$ radicals results in little decarboxylation and preferably proceeds through H-abstraction [27].

The identified TPs can be rationalized based on the above principal reaction mechanisms of $^{\bullet}OH$ radicals towards the functionalities present in VLS molecule. More specifically, three TPs, T-TP1, T-TP3 and T-TP7, with $[M + H]^+$ at m/z 406.2225, 364.1759 and 336.1810 are in common with the TPs detected by g-C_3N_4 catalyst, GCN-TP2, GCN-TP5 and GCN-TP6, respectively. T-TP5 with $[M + H]^+$ at m/z 380.1706 differs 16 amu from T-TP3 and the suggested formula $C_{20}H_{22}O_3N_5^+$ implied a hydroxylated derivative. T-TP2 with $[M + H]^+$ at m/z 362.1599 is 2 amu less than T-TP3 and the suggested formula $C_{20}H_{20}O_2N_5^+$ point out the formation of a double bond or a ring on the TP structure. T-TP2 was assigned to a cyclization product, with tetrazole –NH group participating in the cyclization after the abstraction of labile hydrogen by $^{\bullet}OH$ radicals.

Similarly, T-TP8 and T-TP6 were assigned to a hydroxy and keto derivative of T-TP2 presenting $[M + H]^+$ at m/z 378.1550 and 376.1392 with chemical formulas of $C_{20}H_{20}O_3N_5^+$ and $C_{20}H_{18}O_3N_5^+$, respectively. Another evidence for the above tetra cyclic TPs (T-TP8, T-TP6) is the higher retention times compared to the precursor TPs due to the less polar character. Such cyclization derivatives are reported for VLS during oxidation by persulfate activation to $SO_4^{\bullet-}$ [17], but they have been identified also for the structurally related drug irbesartan, during photolysis [28] and hypochlorite treatment [29].

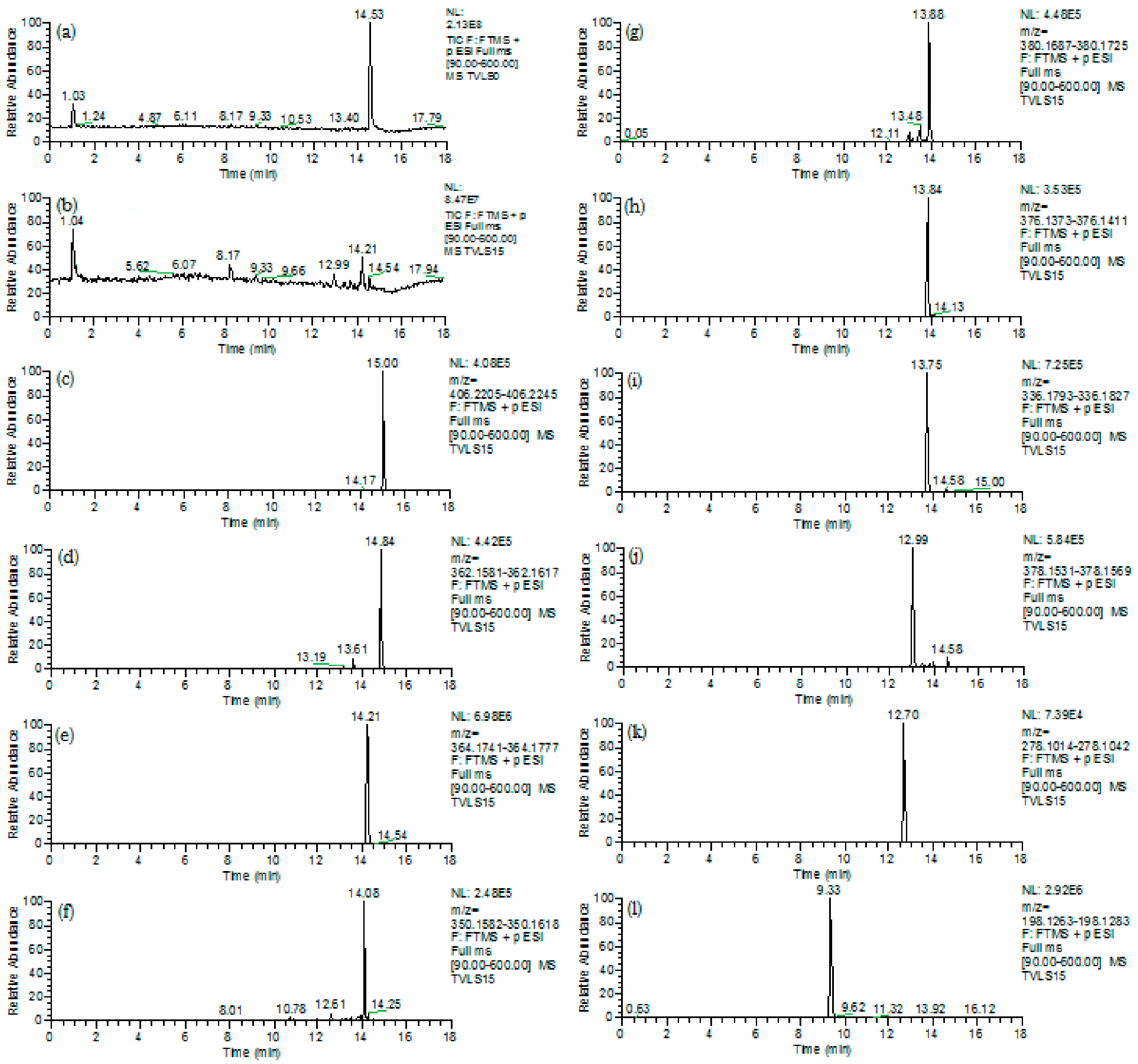

Figure 5. (**a**–**l**). LC-HR-MS TPs accurate-mass extracted chromatograms of TiO_2-photocatalytically treated (reaction time 15 min) VLS aqueous solutions.

Amide bond cleavage and subsequent cyclization was considered for the formation of T-TP4 with $[M + H]^+$ 350.1600 and $C_{19}H_{20}O_2N_5^+$ as the suggested chemical formula. Further oxidation led to the formation of T-TP9 presenting $[M + H]^+$ 278.1018 and $C_{15}H_{12}ON_5^+$. Finally, the rupture of tetrazole ring and N-substituents led to the formation of T-TP10 with a formula of $C_{14}H_{16}N^+$ bearing $[M + H]^+$ 198.1273. The above assignments can be further rationalized considering their evolution profiles (Figure 6). T-TP1, T-TP3-TP5, and T-TP7 maximized at 15 min and can be considered as primary products, while all cyclization derivatives (T-TP2, T-TP6, T-TP8 and T-TP9) peak up at longer treatment times and are considered as secondary TPs. Finally, TP10 peak up at 90 min and can be considered as late stage product. The corresponding TOC removal after 240 min of irradiation under the current experimental conditions was 15%.

Table 2. UPLC-ESI(+)-HR-MS data (pseudo-molecular ions $(M + H)^+/(M + Na)^+$; chemical formula; mass error Δ(ppm); and ring-double bond equivalents, RDB) for VLS transformation products by TiO_2 photocatalytic oxidation.

TPs	$(M + H)^+/(M + Na)^+$	Formula	Δ(ppm)	RDB
T-TP1	406.2225 428.2044	$C_{23}H_{28}O_2N_5$ $C_{23}H_{27}O_2N_5Na$	−3.081	12.5
T-TP2	362.1599 384.1419	$C_{20}H_{20}O_2N_5$ $C_{20}H_{19}O_2N_5Na$	−3.345	13.5
T-TP3	364.1759 386.1575	$C_{20}H_{22}O_2N_5$ $C_{20}H_{21}O_2N_5Na$	−2.475	12.5
T-TP4	350.1600 372.1418	$C_{19}H_{20}O_2N_5$ $C_{19}H_{19}O_2N_5Na$	−3.374	12.5
T-TP5	380.1706 402.1523	$C_{20}H_{22}O_3N_5$ $C_{20}H_{21}O_3N_5Na$	−2.962	12.5
T-TP6	376.1392 398.1211	$C_{20}H_{18}O_3N_5$ $C_{20}H_{17}O_3N_5Na$	−3.180	14.5
T-TP7	336.1810 358.1629	$C_{19}H_{22}ON_5$ $C_{19}H_{21}ON_5Na$	−2.727	11.5
T-TP8	378.1550 400.1368	$C_{20}H_{20}O_3N_5$ $C_{20}H_{19}O_3N_5$	−2.819	13.5
T-TP9	278.1028 300.0847	$C_{15}H_{12}ON_5$ $C_{15}H_{11}ON_5$	−2.864	12.5
T-TP10	198.1273	$C_{14}H_{16}N$	−1.848	7.5

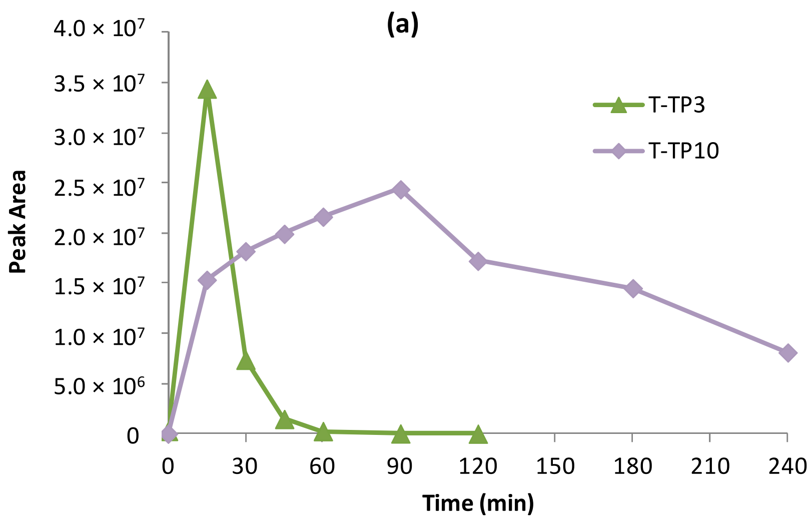

Figure 6. *Cont.*

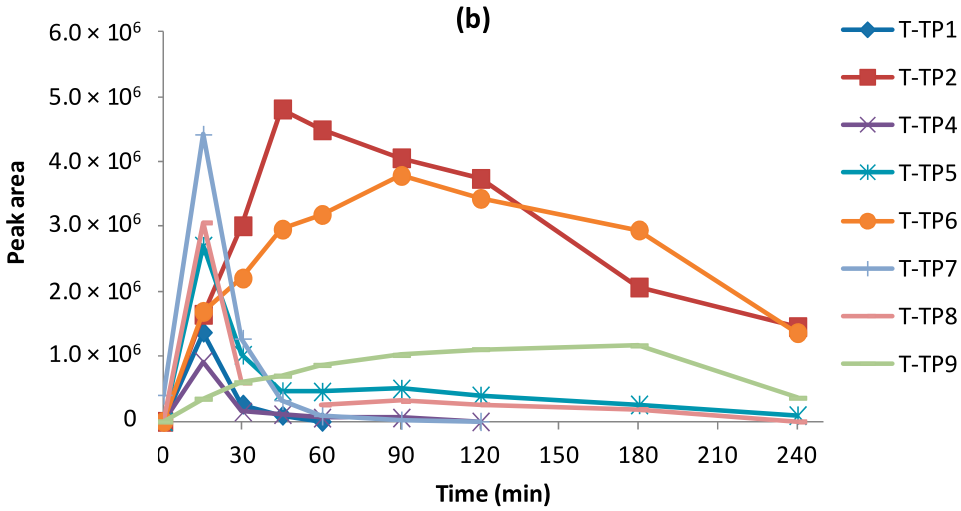

Figure 6. Evolution profiles of major (**a**) and minor (**b**) VLS TPs by TiO_2 photocatalytic oxidation process.

Based on the structure assignments and TPs evolution profiles, the tentative transformation pathways are summarized in Figure 7. In conclusion, the VLS TiO_2 photocatalytic degradation process followed four major pathways (Figure 7): (a) N-lateral chain oxidation; (b) cyclization; (c) hydroxylation; and (d) cleavage of the amide bond. Two main differences can be noted compared to the g-C_3N_4 process., i.e., the presence of cyclization TPs and the absence of hydroxy-derivatives of VLS.

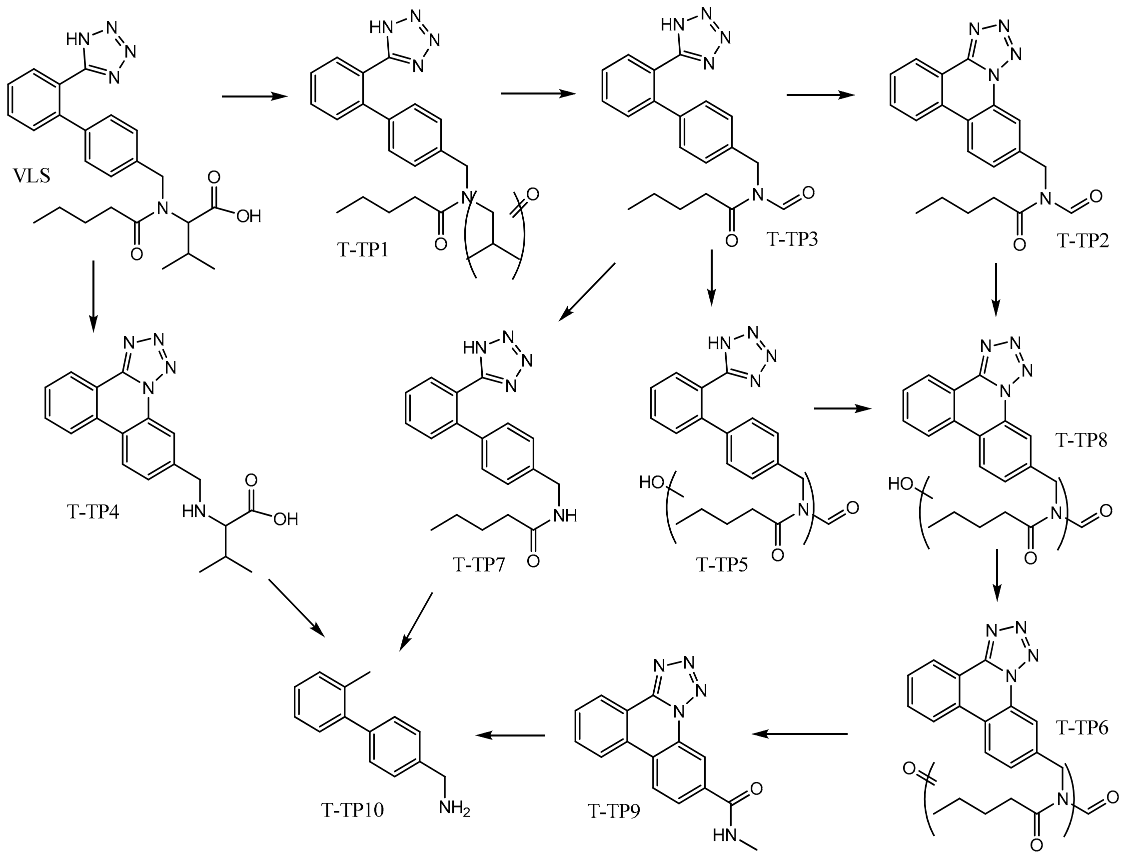

Figure 7. The proposed degradation pathways of valsartan by TiO_2 photocatalytic oxidation.

3. Materials and Methods

3.1. Materials and Chemicals

Valsartan (98%) was purchased from Sigma—Aldrich. Methanol (MeOH) and water of LC-MS grade was supplied by Fisher Scientific (Loughborough, UK). Urea (99.5%) was obtained from Acrōs Organics (Geel, Belgium). Oasis HLB (divinylbenzene/N-vinylpyrrolidone copolymer) cartridges (60 mg, 3 mL) from Waters (Mildford, MA, USA) were used for the extraction of TPs. Two different semiconductor materials were used. The first included the aeroxide TiO_2-P25 supplied by the Evonik-Degussa Corporation (BET specific surface area (SSA) 50 ± 15 m^2g^{-1}, 80% anatase, 20% rutile, average primary particle size 21 nm, E_g = 3.15 eV). The second, the g-C_3N_4 catalyst, was synthesized with the use of urea as a precursor compound. The urea was placed in an aluminum crucible and was dried in 90 °C for 24 h. After that, was calcinated in air at 500 °C with heating rate of 10 °C min^{-1}. The furnace was cooled down naturally and the collected yellow color solid was ground well into a powder in an agate mortar. The main physicochemical properties of g-C_3N_4 were as follows: specific surface area 35 m^2g^{-1}, particle size of 25 nm, E_g = 2.82 eV [30].

3.2. Photocatalytic Treatment Experiments

A solar simulator (Suntest XLS+, Atlas, Linsengericht, Germany) equipped with a xenon lamp (2.2 kW) was used for performing photocatalytic experiments UV–vis irradiation (simulated solar light, $\lambda > 290$ nm) using a 290 nm cut-off glass filter. Before illumination, 0.1 mL of valsartan standard solution in methanol (C = 5000 mgL^{-1}) was added to 100 mL bidistilled water in order to achieve an initial concentration (C_0) of 5 mgL^{-1} and then 100 mgL^{-1} of photocatalyst was added under stirring (600 rpm). The suspension was loaded in Pyrex reactor (250 mL) and kept in the dark for 30 min in order to achieve the adsorption equilibrium. Adsorption experiments took place in dark conditions showed adsorption percentages of 14.3% and 1.8% for TiO_2 and g-C_3N_4, respectively. The above experimental conditions were selected in order to obtain not so fast kinetics and to facilitate the identification and the follow-up of the transformation products. A constant radiation intensity (500 W m^{-2}) was kept throughout the experiments, while the temperature was kept at 23 ± 1 °C by a water circuit in the double-jacked photoreactor and air circulation. Samples $\approx$ 2 mL were periodically withdrawn and filtered by 0.22 μm filters for further LC-MS and total organic carbon (TOC) analysis using a TOC-L CSH/CSN (Shimadzu, Kyoto, Japan) analyzer.

3.3. Identification of Transformation Products by Liquid Chromatography-High Resolution Mass Spectrometry

The analysis of the photocatalytically treated aqueous samples was performed by accurate mass high resolution liquid chromatography-mass spectrometry (LTQ-Orbitrap XL, Thermo Fisher Scientific, Inc., GmbH, Bremen, Germany). The instrument combines a UHPLC Accela LC system (Accela LC pump, Accela Autosampler) and a linear–ion–trap–Orbitrap™ hybrid mass spectrometer. ESI ionization was performed in both positive and negative mode. The analysis was performed according to the following conditions: gradient elution with 0.1% formic acid in LC-MS grade water (mobile phase A) and 0.1% formic acid in LC-MS grade methanol (mobile phase B); Speedcore-Fortis diphenyl (2.1 mm × 50 mm, 2.6 μm particle size) column operated at 35 °C; gradient elution started with 95% A (2 min) and progressed according to 90% A, 70% A and 50% A in 3, 5 and 10 min, respectively, finally returned to 80% A and initial conditions in 15 and 18 min, respectively, with 1 min column re-equilibration time; flow rate 0.25 mL/min; injection volume 20 μL. The mass range was scanned within 90−600 m/z, while mass spectra data were recorded using a resolving power of 60.000 and 15.000 in FT-MS mode for MS and MS^2/MS^3 scans, respectively. A mass accuracy of ±5 ppm was adopted by performing external calibration of the Orbitrap mass analyzer. The processing of data was performed by Thermo Xcalibur 2.1 software (Thermo Electron, San Jose, CA, USA).

3.4. Determination of $^{\bullet}$OH Radicals by Fluorescence Measurements

The terephthalic acid (TA) (98%, Sigma-Aldrich, St. Louis, MO, USA) method was used for the quantification of the generated $^{\bullet}$OH radicals. Aqueous solutions (100 mL) of TA (5×10^{-4} M) and NaOH (2×10^{-3} M, 99% Riedel de Haẽn, Seelze, Germany) were prepared and then the catalysts were added to the solutions, which were placed to the reactor. The experimental conditions remained the same with the photocatalytic experiments. Samplings (5 mL) were performed at different time intervals and samples were filtered with 0.22 μm filters. The fluorescence peak at 425 nm (excitation wavelength at 310 nm) is ascribed to 2-hyroxyterephthalic acid (TAOH). A calibration curve plotting the fluorescence intensity of standard TAOH took place for measuring the concentrations of $^{\bullet}$OH.

4. Conclusions

The photocatalytic degradation pathways of the valsartan pharmaceutical were studied in the presence of g-C_3N_4 and TiO_2 catalysts using LC-MS-Orbitrap high resolution accurate mass spectrometry. Ten transformation products were identified for each catalyst, but only three of them are in common, suggesting the different degradation pathways followed. For g-C_3N_4, the major paths included decarboxylation and subsequent oxidation, hydroxylation, and cleavage of C–N bond. On the other hand, in the presence of TiO_2 cyclization, TPs are abundant and hydroxylation occurs in the first stage products due to the higher production of $^{\bullet}$OH radicals. Thus, the generation of transformation products is greatly influenced by the catalytic mechanism suggesting that their identification is highly significant in photocatalytic processes or in other oxidoreductive processes in the environment. In the case of TiO_2, all transformation products were also degraded for more than 60%, but, in the presence of g-C_3N_4, some products still increased their concentrations within the time framework of 240 min. Overall, this work demonstrated the importance of identifying the TPs for the assessment of photocatalytic processes since they can be more persistent and/or toxic depending on the catalyst used.

Author Contributions: Conceptualization, I.K. and F.B.; methodology, F.B.; formal analysis, I.K. and F.B.; investigation, F.B.; resources, I.K.; writing—original draft preparation, F.B. and I.K.; writing—review and editing, F.B. and I.K.; visualization, F.B.; supervision, I.K.; funding acquisition, F.B. and I.K. All authors have read and agreed to the published version of the manuscript.

Funding: This research work was funded by the Hellenic foundation for Research and Innovation (HFRI) under the HFRI PhD fellowship grant (Fellowship number: 269, Project number: 82697).

Institutional Review Board Statement: Not applicable.

Informed Consent Statement: Not applicable.

Data Availability Statement: Data are contained within the article.

Acknowledgments: The authors would like to thank the unit of environmental, organic and biochemical high resolution–Orbitrap–LC–MS analysis of the University of Ioannina for providing access to the instrumentation facilities.

Conflicts of Interest: The authors declare no conflict of interest.

References

1. Taoufik, N.; Boumya, W.; Janani, F.Z.; Elhalil, A.F.Z.; Mahjoubi, N.B. Removal of emerging pharmaceutical pollutants: A systematic mapping study review. *J. Environ. Chem. Eng.* **2020**, *8*, 104251. [CrossRef]
2. Kosma, C.I.; Lambropoulou, D.A.; Albanis, T.A. Investigation of PPCPs in wastewater treatment plants in Greece: Occurrence, removal and environmental risk assessment. *Sci. Total Environ.* **2014**, *466–467*, 421–438. [CrossRef] [PubMed]
3. Kosma, C.I.; Nannou, C.I.; Boti, V.I.; Albanis, T.A. Psychiatrics and selected metabolites in hospital and urban wastewaters: Occurrence, removal, mass loading, seasonal influence and risk assessment. *Sci. Total Environ.* **2019**, *659*, 1473–1483. [CrossRef]
4. Antonopoulou, M.; Kosma, C.; Albanis, T.; Konstantinou, I. An overview of homogeneous and heterogeneous photocatalysis applications for the removal of pharmaceutical compounds from real or synthetic hospital wastewaters under lab or pilot scale. *Sci. Total Environ.* **2021**, *765*, 144163. [CrossRef]

5. Papageorgiou, M.; Zioris, I.; Danis, T.; Bikiaris, D.; Dimitra Lambropoulou, D. Comprehensive investigation of a wide range of pharmaceuticals and personal care products in urban and hospital wastewaters in Greece. *Sci. Total Environ.* **2019**, *694*, 133565. [CrossRef] [PubMed]
6. Nödler, K.; Hillebrand, O.; Idzik, K.; Strathmann, M.; Schiperski, F.; Zirlewagen, J.; Licha, T. Occurrence and fate of the Angiotensin II receptor antagonist transformation product Valsartan acid in the water cycle-A comparative study with selected β-blockers and the persistent anthropogenic wastewater indicators carbamazepine and acesulfame. *Water Res.* **2013**, *47*, 6650–6659. [CrossRef]
7. Brunetto, M.R.; Contreras, Y.; Clavijo, S.; Torres, D.; Delgado, Y.; Ovalles, F.; Ayala, C.; Gallignani, M.; Estela, J.M.; Martin, V.C. Determination of losartan, telmisartan and valsartan by direct injection human urine into a column-switching liquid chromatographic system with fluorescence detection. *J. Pharm. Biomed. Anal.* **2009**, *50*, 194–199. [CrossRef]
8. Zhou, S.; Paolo, C.D.; Wu, X.; Shao, Y.; Seiler, T.B. Optimization of screening-level risk assessment and priority selection of emerging pollutants–The case of pharmaceuticals in European surface water. *Environ. Int.* **2019**, *128*, 1–10. [CrossRef]
9. Castro, C.; Rodriguez, I.; Ramil, M.; Cela, R. Selective determination of sartan drugs in environmental water samples by mixed-mode solid-phase extraction and liquid chromatography tandem mass spectrometry. *Chemosphere* **2019**, *224*, 562–571. [CrossRef]
10. Pena-Guzman, C.; Ulloa-Sanchez, S.; Mora, K.; Helena-Bustos, R.; Lopes-Barrera, E.; Alvarez, J.; Rodriguez-Pinzon, M. Emerging pollutants in the urban water cycle in Latin America: A review of the current literature. *J. Environ. Manag.* **2019**, *237*, 408–423. [CrossRef]
11. Kosma, C.I.; Lambropoulou, D.A.; Albanis, T.A. Occurrence and removal of PPCPs in municipal and hospital wastewaters in Greece. *J. Hazard. Mater.* **2010**, *179*, 804–817. [CrossRef] [PubMed]
12. Kosma, C.I.; Lambropoulou, D.A.; Albanis, T.A. Comprehensive study of the antidiabetic drug metformin and its transformation product guanylurea in Greek wastewaters. *Water Res.* **2015**, *70*, 436–448. [CrossRef] [PubMed]
13. Konstantinou, I.K.; Albanis, T.A. Photocatalytic transformation of pesticides in aqueous titanium dioxide suspensions using artificial and solar light: Intermediates and degradation pathways. *Appl. Catal. B Environ.* **2003**, *42*, 319–335. [CrossRef]
14. Kanakaraju, D.; Glass, B.D.; Oelgemöller, M. Advanced oxidation process-mediated removal of pharmaceuticals from water: A review. *J. Environ. Manag.* **2018**, *219*, 189–207. [CrossRef]
15. Mamba, G.; Mishra, A.K. Graphitic carbon nitride (g-C_3N_4) nanocomposites: A new and exciting generation of visible light driven photocatalysts for environmental pollution remediation. *Appl. Catal. B Environ.* **2016**, *198*, 347–377. [CrossRef]
16. Wang, Y.; Wang, X.; Antonietti, M. Polymeric Graphitic Carbon Nitride as a Heterogeneous Organocatalyst: From Photochemistry to Multipurpose Catalysis to Sustainable Chemistry. *Angew. Chem. Int. Ed.* **2012**, *51*, 68–89. [CrossRef]
17. Arvaniti, O.S.; Bairamis, F.; Konstantinou, I.; Mantzavinos, D.; Frontistis, Z. Degradation of antihypertensive drug valsartan in water matrices by heat and heat/ultrasound activated persulfate: Kinetics, synergy effect and transformation products. *CEJ Adv.* **2020**, *4*, 100062. [CrossRef]
18. Martinez-Pachon, D.; Ibanez, M.; Hernandez, F.; Torres-Palma, R.A.; Moncayo-Lasso, A. Photo-electro-Fenton process applied to the degradation of valsartan: Effect of parameters, identification degradation routes and mineralization in combination with a biological system. *J. Environ. Chem. Eng.* **2018**, *6*, 7302–7311. [CrossRef]
19. Serna-Galvis, E.A.; Isaza-Pineda, L.; Moncayo-Lasso, A.; Ibanez, M.; Torres-Palma, R.A. Comparative degradation of two highly consumed antihypertensives in water by sonochemical process. Determination of the reaction zone, primary degradation products and theoretical calculations on the oxidative process. *Ultrason. Sonochem.* **2019**, *58*, 104635. [CrossRef]
20. Diehle, M.; Gebhardt, W.; Pinnekamp, J.; Schäffer, A.; Linnemann, V. Ozonation of valsartan: Structural elucidation and environmental properties of transformation products. *Chemosphere* **2019**, *216*, 437–448. [CrossRef]
21. Park, H.; Kim, H.I.; Moon, G.H.; Choi, W. Photoinduced charge transfer processes in solar photocatalysis based on modified TiO_2. *Energy Environ. Sci.* **2016**, *9*, 411–433. [CrossRef]
22. Bennett, J.E.; Summers, R. Product studies of the mutual termination reactions of sec-alkylperoxy radicals: Evidence for non-cyclic termination. *Can. J. Chem.* **1974**, *52*, 1377–1379. [CrossRef]
23. Von Sonntag, C.; Schuchmann, H.P. The Elucidation of Peroxyl Radical Reactions in Aqueous Solution with the Help of Radiation-Chemical Methods. *Angew. Chem. Int. Ed. Engl.* **1991**, *30*, 1229–1253. [CrossRef]
24. Hu, J.; Wang, J.; Nguyen, T.H.; Zheng, N. The chemistry of amine radical cations produced by visible light photoredox catalysis. *Beilstein J. Org. Chem.* **2013**, *9*, 1977–2001. [CrossRef]
25. Dey, G.R.; Naik, D.B.; Kishore, K.; Moorthy, P.N. Pulse radiolysis study of 5-amino tetrazole in aqueous solutions. Radiat. *Phys. Chem.* **1996**, *47*, 559–562.
26. Hayon, E.; Ibata, T.; Lichtin, N.N.; Simic, M. Sites of attack of hydroxyl radicals on amides in aqueous solution. *J. Am. Chem Soc.* **1970**, *92*, 3898–3903. [CrossRef]
27. Madhavan, V.; Levanon, H.; Neta, P. Decarboxylation by SO_4^- Radicals. *Radiat. Res.* **1978**, *76*, 15–22. [CrossRef]
28. Shah Ravi, P.; Sahu, A.; Singh, S. Identification and characterization of degradation products of irbesartan using LC–MS/TOF, MSn on-line H/D exchange and LC–NMR. *J. Pharm. Biomed. Anal.* **2010**, *51*, 1037–1046. [CrossRef]
29. Romanucci, V.; Siciliano, A.; Guida, M.; Libralato, G.; Luongo, G.; Previtera, L.; Di Fabio, G.; Zarrelli, A.; Saviano, L. Disinfection by-products and ecotoxic risk associated with hypochlorite treatment of irbesartan. *Sci. Total Environ.* **2020**, *712*, 135625. [CrossRef]
30. Bairamis, F.; Konstantinou, I.; Petrakis, D.; Vaimakis, T. Enhanced Performance of Electrospun Nanofibrous TiO_2/g-C_3N_4 Photocatalyst in Photocatalytic Degradation of Methylene Blue. *Catalysts* **2019**, *9*, 880. [CrossRef]